JACS
JOURNAL OF THE AMERICAN CHEMICAL SOCIETY

Article

pubs.acs.org/JACS

Variable Doping Induces Mechanism Swapping in Electrogenerated Chemiluminescence of $Ru(bpy)_3^{2+}$ Core–Shell Silica Nanoparticles

Giovanni Valenti,[†,∥] Enrico Rampazzo,[†,∥] Sara Bonacchi,[†,§] Luca Petrizza,[†] Massimo Marcaccio,[†] Marco Montalti,[†] Luca Prodi,*[,†] and Francesco Paolucci*[,†,‡]

[†]Department of Chemistry "G. Ciamician", University of Bologna, Via Selmi 2, 40126 Bologna, Italy
[‡]ICMATE-CNR Bologna Associate Unit, University of Bologna, Via Selmi 2, 40126 Bologna, Italy

Supporting Information

ABSTRACT: The impact of nanotechnology on analytical science is hardly overlooked. In the search for ever-increasing sensitivity in biomedical sensors, nanoparticles have been playing a unique role as, for instance, ultrabright labels, and unravelling the intimate mechanisms which govern their functioning is mandatory for the design of ultrasentitive devices. Herein, we investigated the mechanism of electrogenerated chemiluminescence (ECL) in a family of core–shell silica–PEG nanoparticles (DDSNs), variously doped with a $Ru(bpy)_3^{2+}$ triethoxysilane derivative, and displaying homogeneous morphological, hydrodynamic, and photophysical properties. ECL experiments, performed in the presence of 2-(dibutylamino)ethanol (DBAE) as coreactant, showed two parallel mechanisms of ECL generation: one mechanism (I) which involves exclusively the radicals deriving from the coreactant oxidation and a second one (II) involving also the direct anodic oxidation of the Ru(II) moieties. The latter mechanism includes electron (hole) hopping between neighboring redox centers as evidenced in our previous studies and supported by a theoretical model we have recently proposed. Quite unexpectedly, however, we found that the efficiency of the two mechanisms varies in opposite directions within the DDSNs series, with mechanism I or mechanism II prevailing at low and high doping levels, respectively. Since mechanism II has an intrinsically lower efficiency, the ECL emission intensity was also found to grow linearly with doping only at relatively low doping levels while it deviates negatively at higher ones. As the ζ-potential of DDSNs increases with the doping level from negative to slightly positive values, as a likely consequence of the accumulating cationic charge within the silica core, we attributed the observed change in the ECL generation mechanism along the DDSN series to a modulation of the electrostatic and hydrophobic/hydrophilic interactions between the DDSNs and the radical cationic species involved in the ECL generation. The results we report therefore show that the ECL intensity of a nanosized system cannot be merely incremented acting on doping, since other parameters come into play. We think that these results could serve as valuable indications to design more efficient ECL nano- and microsized labels for ultrasensitive bioanalysis.

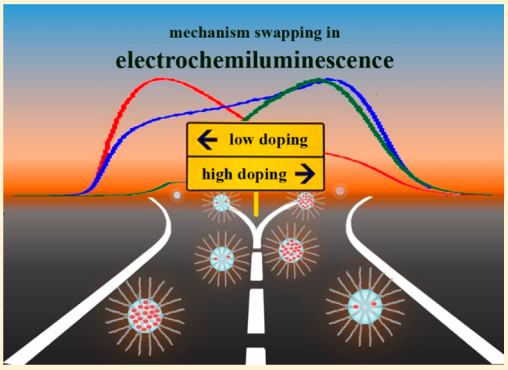

INTRODUCTION

Electrochemiluminescence (ECL) is nowadays a leading technique in bioanalysis. Since the excited species are produced with an electrochemical stimulus rather than with a light excitation source, ECL displays improved signal-to-noise ratio compared to photoluminescence, with minimized effects due to light scattering and luminescence background.[1−4]

In particular, coreactant ECL operating in buffered aqueous solution in the region of positive potentials (oxidative-reduction mechanism) definitively boosted ECL for immunoassay, as confirmed by many research applications[3] and, even more, by the presence of important companies (Roche Diagnostics and MesoScale) which developed commercial hardware for high throughput immunoassays analysis in a market worth billions of dollars each year.[5,6] The commercial success of the ECL technique has fueled research at the fundamental level where new metal complexes, primarily based on Ru(II) and Ir(III), more efficient than the "war horse" $Ru(bpy)_3^{2+}$,[1] and new coreactants have been systematically investigated.[7,8]

In the quest for an ever-increasing sensitivity, ECL can ideally be coupled to nanotechnology and supramolecular chemistry to develop new systems and strategies for analyte determination also in very complex matrices.[9−14] For instance, we have recently shown a supramolecular approach to detect sarcosine, a potential prostate cancer biomarker, in urines, with good sensitivity and very high selectivity.[15] Dye-doped silica nanoparticles (DDSNs),[16−18] semiconductor nanocrystals (QDs),[19−21] or polymer dots[22−25] were also advantageously used as ECL-active systems. In particular, DDSNs present many advantages: they can be obtained with accessible synthetic schemes, are intrinsically hydrophilic, and, thanks to silica chemistry, are prone to bioconjugation. Very bright

Received: August 11, 2016
Published: November 18, 2016

DOI: 10.1021/jacs.6b08239
J. Am. Chem. Soc. 2016, 138, 15935−15942

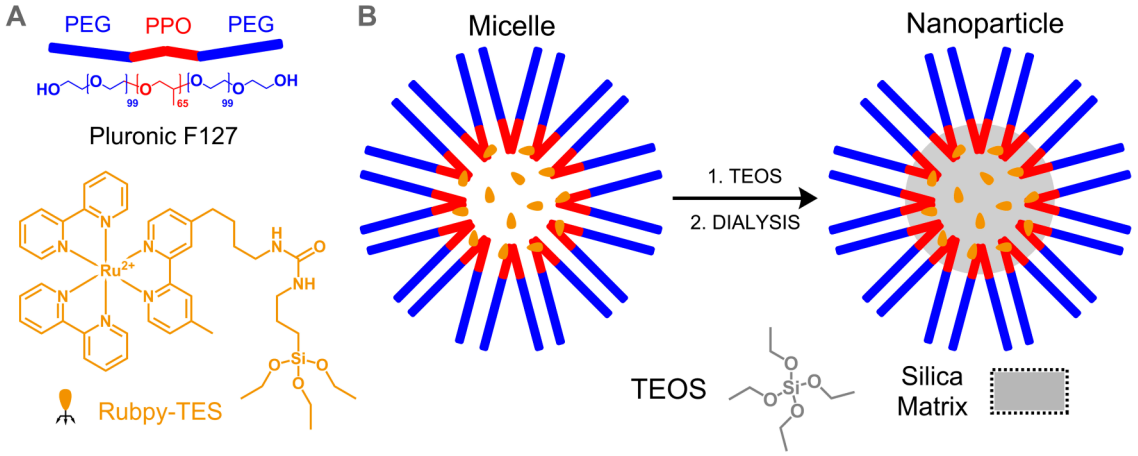

Figure 1. (A) Main synthetic reagents used for the synthesis of core−shell silica−PEG nanoparticles. (B) Schematic representation of the synthetic process.

systems can be obtained with this approach since silica is inert from the photophysical point of view, and DDSNs assume the photophysical properties of the dye(s) molecules accumulated within the nanoparticle.[26] These properties can be extended to ECL, since many ECL-active complexes can dope NPs,[27,28] also exploiting Forster resonance energy transfer (FRET) strategies to tune the emission in association with other fluorescent dyes.[29−31]

In particular, $Ru(bpy)_3^{2+}$, because of its water solubility and positive charge, is an excellent doping agent for silica nanoparticles (NPs), especially with the reverse microemulsion (water-in-oil) synthetic approach.[28,32]

In DDSNs, light emission is influenced by the combination of several factors that make DDSNs complex multichromophoric structures, such as the coexistence of dye populations experimenting with slightly different environments and the occurrence of intraparticle energy transfer processes (mainly resonance energy transfer or quenching). When ECL comes into play, the scenario is even more complicated by the presence of the coreactant−NP interactions, since the coreactant needs to approach the NP surface and to react with the dyes buried within the silica at different extent.[28,33]

Here, we evaluate the influence of the doping level on the ECL generation efficiency in a series of homogeneous core−shell silica−PEG DDSNs covalently doped with a $Ru(bpy)_3^{2+}$ triethoxysilane derivative (Rubpy−TES), obtained with a direct micelle assisted method (Figure 1). We chose this system since the morphological properties are very reproducible (with a core diameter ∼10 nm) and can be obtained in a large Rubpy−TES doping regime (Figure 2). The high colloidal stability of this system in water allowed study of the ECL behavior in suspension, while its core−shell morphology was useful to mimic a doped silica nanoparticle functionalized with a dense organic layer, such as a biomolecular corona. The ζ-potential of DDSNs was found to vary with the Rubpy−TES content, and at the same time, the positive charge accumulating into the silica core resulted in being detrimental to the ECL emission, probably through electrostatic repulsion between the nanoparticle surface and the approaching coreactant cationic intermediates.

EXPERIMENTAL SECTION

Materials. Acetonitrile (MeCN, 99.8%), dichloromethane (DCM, ≥99.8%), Pluronic F127, sodium sulfate (≥99%), tetraethyl

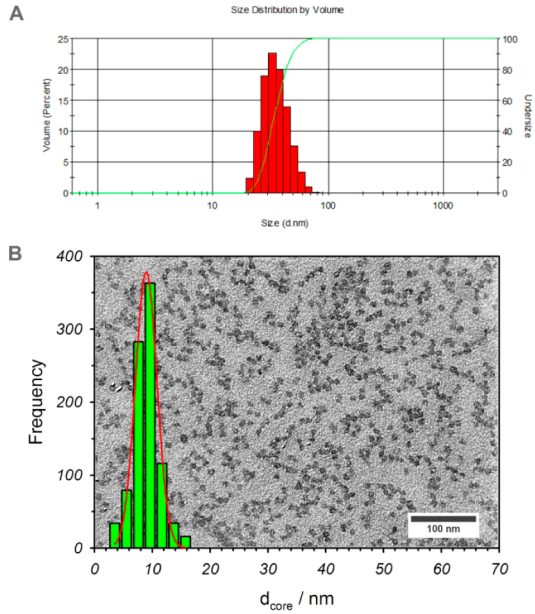

Figure 2. (A) Hydrodynamic diameter distribution of DDSNs (**Ru@NP4**) in water. (B) TEM image and silica core diameter distribution (**Ru@NP4**).

orthosilicate (TEOS, 99.99%), chlorotrimethylsilane (TMSCl, ≥98%), 3-(triethoxysilyl)propyl isocyanate 95%, acetic acid (HOAc, ≥99.7%), ethanol (EtOH), 4,4′-dimethyl-2,2′-bipyridine, Li-diisopropylamine, 1,3-bromopropane, Sephadex SP C-25, and potassium phthalimide were purchased from Sigma-Aldrich. $RuCl_3·3H_2O$, *N*,*N*-diisopropylethylamine (DIPEA, ≥98%), NaCl, and silica on TLC Alu foils (4 × 8 cm^2, with fluorescent indicator 254 nm) were purchased from Fluka, and hydrazine hydroxide was purchased from Merck. UF tubes Amicon Ultra-0.5 mL, cutoff 100 kDa, were purchased from Millipore. Dialysis was performed versus water at room temperature under gentle stirring with regenerated cellulose dialysis tubing (Sigma, mol wt cutoff >12 kDa, av diameter 33 mm). NMR spectra were recorded with a Varian 400 MHz instrument.

Synthesis of the Ru(bpy)−TES Derivative. $Ru(bpy)_2Cl_2·2H_2O$ and 4-(4′-methyl-2,2′-bipyridin-4-yl)-butan-1-amine were synthesized according to previously reported procedures.[34,35]

Preparation of Covalently Doped $Ru(bpy)_3^{2+}$ Core−Shell Silica Nanoparticles. The synthetic scheme, applied for the preparation of core−shell silica−PEG (polyethylene glycol) DDSNs, is shown in Figure 1, while the amounts of reagents used for their preparation are shown in Table 1.

DOI: 10.1021/jacs.6b08239
J. Am. Chem. Soc. 2016, 138, 15935−15942

Table 1. Doping Values, Hydrodynamic Diameters, and ζ-Potentials of the DDSNs Samples Presented in This Work

sample	% mol dye vs mol TEOS	no. dye/NP[a]	Rubpy−TES, μmol	F127, mg	HOAc 1 M, μL	TEOS, μL	TMSCl, μL	NaCl, mg	d_H ± SD, nm	ζ-pot. ± SD, mV
Ru@NP1	0.052	2	8.3	200	3100	360	20	140	19 ± 3	−10.0 ± 1.5
Ru@NP2	0.10	4	1.66	200	3100	360	20	140	18 ± 5	−6.3 ± 0.9
Ru@NP3	0.21	6	3.32	200	3100	360	20	140	27 ± 5	−4.4 ± 1.0
Ru@NP4	0.41	16	6.64	200	3100	360	20	140	22 ± 3	−2.5 ± 1.2
Ru@NP5	0.62	22	4.98	100	1550	180	10	70	35 ± 5	−0.9 ± 0.7
Ru@NP6	0.82	24	6.64	100	1550	180	10	70	32 ± 6	0.9 ± 0.8

[a]Mean values calculated from absorption spectra ($\varepsilon_{(Rubpy-TES)}$ = 14500 cm^{-1} M^{-1}).

Pluronic F127 and Rubpy−TES were solubilized with MeOH (∼1.0 mL) in a 20 mL glass scintillation vial, and the solvent was then removed under vacuum at room temperature. NaCl was added to the solid residue, and the mixture was solubilized at 25 °C under magnetic stirring with acetic acid 1.0 M. TEOS was then added to the resulting aqueous homogeneous solution followed by TMSCl after 180 min. The mixture was kept under stirring for 48 h at 25 °C before dialysis treatments. The dialysis purification steps were carried out versus water on a precise amount of **Ru@NP** solution (1500 μL) finally diluted to a total volume of 10.0 mL with water. The final concentration of the **Ru@NP** solution was measured taking into account the volume after the dialysis.

Photochemical Measurements. UV−vis absorption spectra were recorded at 25 °C by means of PerkinElmer Lambda 45 spectrophotometer. The fluorescence spectra were recorded with a PerkinElmer Lambda LS 55 fluorimeter and with a modular UV−vis−NIR spectrofluorimeter Edinburgh Instruments FLS920 equipped with a photomultiplier Hamamatsu R928P. The latter instrument connected to a PCS900 PC card was used for the time correlated single photon counting (TCSPC) experiments (excitation laser λ = 460 nm). Corrected fluorescence emission and excitation spectra (450 W Xe lamp) were obtained with the same instrument equipped with both a Hamamatsu R928P P photomultiplier tube (for the 500−850 nm spectral range). Quartz cuvettes were used for both absorbance and emission measurements (optical path length of 0.1 and 1 cm). Nanoparticle solutions were diluted with Milli-Q water. Luminescence quantum yields (uncertainty ±15%) were recorded on air-equilibrated solutions using $Ru(bpy)_3^{2+}$ as reference dye.[36] Corrections for instrumental response, inner filter effects, and phototube sensitivity were performed.[37]

Trasmission Electron Microscopy (TEM) Images. TEM images of DDSNs were obtained with a Philips CM 100 microscope, operating at 80 kV, and using 3.05 mm copper grids (Formvar support film, 400 mesh). A drop of DDSNs solution diluted with water (1:50) was placed on the grid and then dried under vacuum. The TEM images showing the denser silica cores were analyzed with ImageJ software, considering a few hundred nanoparticles. The obtained histogram was fitted according to a Gaussian distribution obtaining the average diameter for the silica nanoparticles core.

Dynamic Light Scattering (DLS) Experiments. DDSN hydrodynamic diameter (d_H) distributions were obtained in water at 25 °C with a Malvern Nano ZS DLS instrument equipped with a 633 nm laser diode. Samples were treated with 0.22 μm RC filters and then housed in disposable polystyrene cuvettes of 1 cm optical path length, using water as solvent. The width of DLS hydrodynamic diameter distribution is indicated by PdI (polydispersion index). In the case of a monomodal distribution (Gaussian) calculated by means of cumulant analysis, PdI = $(\sigma/Z_{avg})^2$, where σ is the width of the distribution and Z_{avg} is average diameter of the particles population, respectively. DLS measurements showed no aggregation of the Ru@NPs even after several months.

ζ-Potential Experiments. DDSN ζ-potential values were determined using a Malvern Nano ZS instrument. Samples were housed in a disposable polycarbonate folded capillary cell (750 μL, 4 mm optical path length). Electrophoretic determination of ζ-potential was made under Smoluchowski approximation in acqueous media at moderate electrolyte concentration. Measurements conditions: ζ-potential ± SD (n = 6), [NPs] = 2 μM, [PB] = 1 mM, [KCl] = 1 mM, pH 7.4, 25 °C.

Electrochemical and ECL Measurements. ECL and electrochemical measurements were carried out with an AUTOLAB electrochemical station (Ecochemie, Mod. PGSTAT 30). Nanoparticle suspension was diluted with a phosphate buffer (PB, pH = 7.4). For ECL generation, 30 mM DBAE (2-(dibutylamino)ethanol) was added as oxidative coreactant. ECL was obtained in single oxidative steps (pulse steps or sweep steps) by generating the oxidized forms of the amine according to known heterogeneous ECL mechanisms.[38] The working electrode consisted of a platinum side-oriented 2 mm diameter disk sealed in glass or indium tin oxide (ITO) (from Kuramoto Seisakusho Co. Ltd. Tokyo, Japan) while the counter electrode was a platinum spiral and the reference electrode was a Ag/AgCl (3 M) electrode. The ECL signal generated by performing the potential step program was measured with a photomultiplier tube (PMT, Hamamatsu R4220p) placed, at a constant distance, under the cell and inside a homemade dark box. A voltage in the range 550−750 V was supplied to the PMT. The light/current/voltage curves were recorded by collecting the preamplified PMT output signal (by a ultralow noise Acton research model 181) with the second input channel of the ADC module of the AUTOLAB instrument.

RESULTS AND DISCUSSION

Aiming at the investigation of the mechanism of ECL emission operating in DDSNs and its dependence on the doping level, we needed a synthetic approach yielding a set of DDSNs with homogeneous morphological properties and very high colloidal stability in a large $Ru(bpy)_3^{2+}$ doping range. For this reason, we chose a one pot direct micelle assisted method producing core−shell silica−PEG nanoparticles, where Pluronic F127 micelles were used as templates. Using this method, we had previously developed core−shell NPs hosting an apolar, water insoluble, Ir(III) complex to investigate its ECL emission in aqueous buffer,[27] and other fluorescent probes systems[38,39] also for imaging applications.[40−42]

The synthetic scheme and the morphological properties of the nanoparticles are summarized in Figures 1 and 2. The DDSNs hard silica diameter (∼10 nm) and their hydrodynamic diameter (∼25 nm, due the presence of a PEG shell) were measured by TEM and DLS analysis, respectively (Figure 2), and are summarized in Table 1 (see also Tables S1 and S2 and Figures S1−S6 and S7−S12 in the Supporting Information). The colocalization of these structures was already demonstrated by other experimental techniques (NMR,[29] AFM, and TGA coupled to UF experiments[27]).

We obtained a set of six DDSNs samples, doped with an increasing amount of Rubpy−TES spanning from 0.05% to 0.8% (mol Rubpy−TES/mol TEOS × 100, **Ru@NP1−Ru@NP6**, Table 1). These doping regimes correspond to an average of 2 ÷ 24 ruthenium complexes per nanoparticle (as measured by absorption UV−vis measurements, see below for details), with the last values being very close to the loading limit in these

DOI: 10.1021/jacs.6b08239
J. Am. Chem. Soc. 2016, 138, 15935−15942

experimental conditions. Dye leaching was prevented by the covalent link of $Ru(bpy)_3^{2+}$ dye to the silica matrix via a triethoxysilane group.

Despite the morphological homogeneity evidenced by TEM and DLS analysis, we found that the inclusion of Rubpy−TES mitigated the negative nanoparticle ζ-potential (Table 1, Table S3, and Figure 3), without affecting the colloidal stability, with a

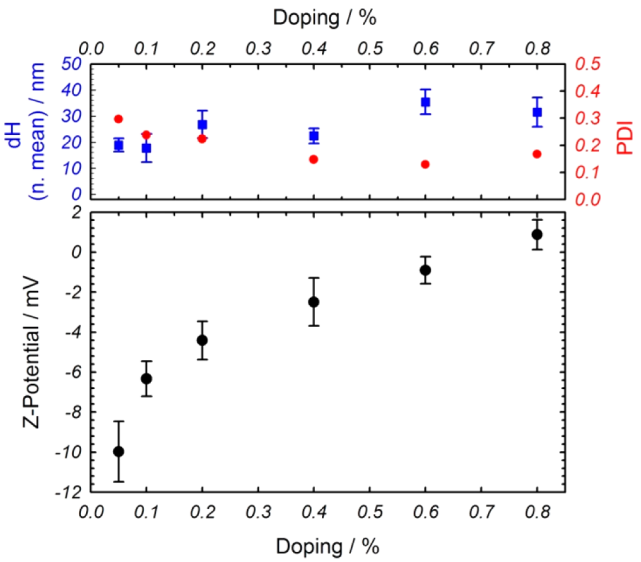

Figure 3. ζ-Potential (lower panel), hydrodynamic diameter (by number mean), and PDI (polydispersion Index) (upper panel) of samples **Ru@NP1−6** vs Rubpy−TES doping percentage. Conditions: [**Ru@NP**] = 4 μM, [KCl] = 1 mM, [phosphate buffer] = 1 mM, pH 7.0, T = 25 °C (all samples were filtered with a 200 nm RC syringe filter). Hydrodynamic diameter and ζ-potential values are reported in Table 1; error bars were calculated as standard deviations of 10 measurements.

trend matching the doping level. This demonstrated that steric stabilization was probably mainly responsible for the colloidal stability of these kinds of DDSNs. This result was in agreement with the tuning of ζ-potential obtained with NIR emitting fluorescent silica nanoprobes for sentinel lymph nodes mapping by the introduction of charged negative groups in the silica core.[40]

Photophysical Properties and Characterization. The average number of dyes embedded in the nanoparticle core was calculated by measuring the concentration of Rubpy−TES in each suspension by absorption spectroscopy, and dividing these values by the nanoparticles concentration, determined as previously reported.[29]

The absorption spectra reported in Figure 4 (see also Figure S13) show that the Rubpy−TES dyes in every sample exhibited very similar polarity environments and ground state conditions. The saturation trend we observed (Figure 4, inset) indicates that sample **Ru@NP6** has a Rubpy−TES content very close to the doping limit of the silica core for this dye.

The triethoxysilane functionalization of Rubpy−TES and the extended dialysis purification assured the absence of free dye in solution, making DDSNs the sole emitting systems in the samples. The trend of the quantum yields and of the average excited state lifetimes in aerated water solutions (λ_{ex} = 460 nm, Figure 5) showed a marked influence of dye inclusion in the silica matrix, when compared to the reference luminophore $Ru(bpy)_3^{2+}$ in the same conditions (Φ = 0.03; τ = 370 ns), a

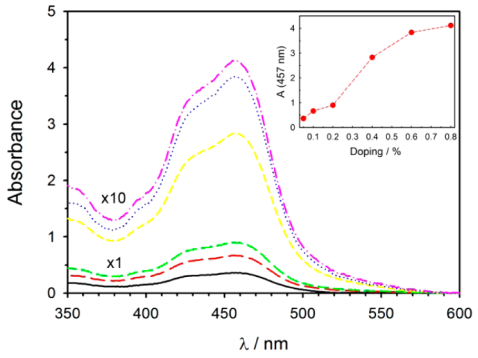

Figure 4. Absorption spectra of samples **Ru@NP** (**1**, black; **2**, red; **3**, green; **4**, yellow; **5**, blue; **6**, pink). Conditions: water, [**Ru@NP**] = 10 μM filtered with a RC 200 μm filter. Samples **Ru@NP1−3**, cuvettes with optical path 1 cm; samples **Ru@NP4−6**, cuvettes with optical path 0.1 cm. Inset: absorbance at 457 nm vs % doping.

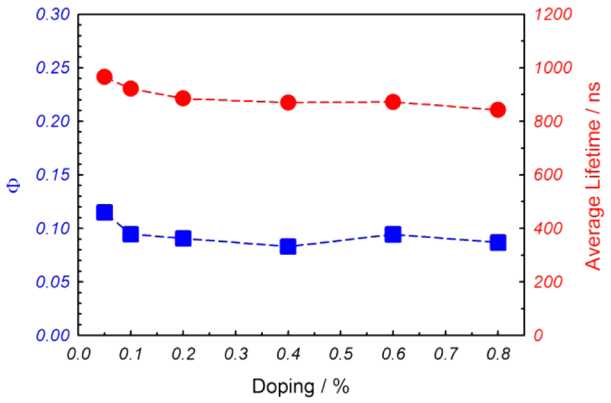

Figure 5. Luminescence quantum yields (blue) and average excited state lifetimes (red) values for samples **Ru@NP1−6** in aerated conditions (water, λ_{ex} = 460 nm). For reference compound $Ru(bpy)_3^{2+}$: Φ = 0.03; τ = 370 ns.

behavior that was imputable to the reduced diffusion of oxygen in the silica core.[43]

Both the quantum yields and the average excited state lifetimes of the samples showed only a slight decrease moving from **Ru@NP1** to **Ru@NP6** (Figure 5), evidencing negligible self-quenching phenomena along the DDSN series. In particular, these values confirm the reduced diffusion of oxygen in the silica core[43] and can be considered quite homogeneous with consideration of their measurement experimental error (∼15%), and they evidenced how the synthetic method we adopted produced similar samples independent from the doping degree, also from the photophysical point of view.

Electrochemical and ECL Behavior vs Doping. Taking advantage of their high colloidal stability, we investigated the electrochemical and ECL properties of **Ru@NP1−6** in aqueous buffer solution using the approach based on the use of a coreactant.[44] In a comparison to the previous experimental setup where nanoparticles were linked to an electrode surface through alkanethiols linkers,[28] the present approach had the main advantage of a simplified synthetic scheme and allowed us to single out the effect of doping on the ECL intensity, without the complications associated with the electrochemically induced reactivity of the self-assembled monolayer.[28]

The electrochemical and ECL measurements were carried out in a phosphate buffer (PB, pH = 7.4), using 2-(dibutylamino)ethanol (DBAE, 30 mM) as "oxidative-reduc-

DOI: 10.1021/jacs.6b08239
J. Am. Chem. Soc. 2016, 138, 15935−15942

tion" coreactant,[7] and evidenced strong effects associated with the doping level on both voltammetric and ECL behavior. Preliminary experiments were also carried out with other coreactants such as tripropylamine (TPA) and oxalate which however gave much less intense ECL signals and were not further used (see Figure S14). The reason for the much lower efficiency obtained with such coreactants is not clear although it may possibly be associated with either their different hydrophilicity or charge of the species intervening in the ECL generation mechanism.

The current−potential and ECL−potential profiles of 80 μM **Ru@NP1** (Ru/NP = 2) are shown in Figure 6a,b.

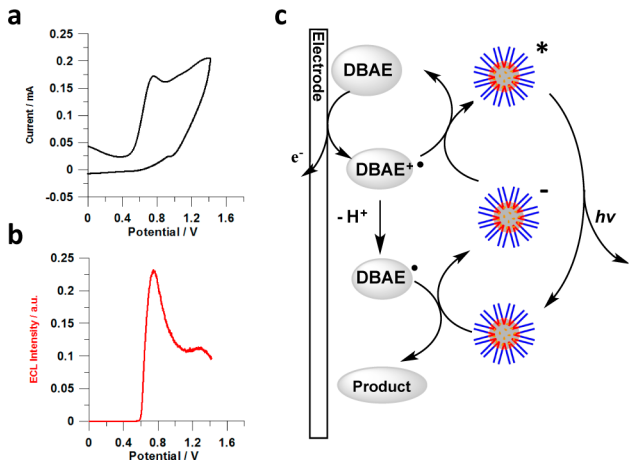

Figure 6. Cyclic voltammetry (black trace panel a) and ECL intensity (red trace panel b) vs potential curves of **Ru@NP1** (Ru/NP = 2) in 100 mM PB solutions with 30 mM DBAE as coreactant: scan rate 0.1 V s^{-1} (*E* vs SCE), PMT bias 750 V. (c) Schematic representation for mechanism I in the "oxidative-reduction" coreactant homogeneous ECL generation of DDSN and DBAE.

The CV curve displays a well-defined anodic peak at 0.8 V associated with the DBAE oxidation while the blurred peak observed at more positive potentials would correspond to the oxidation of the Ru(II) moieties embedded in the NPs. A $Ru(bpy)_3^{2+}$ solution investigated in the same conditions and with the same nominal dye concentration (320 μM, Figure S15) shows in fact a well-defined peak around 1.2 V, associated with the luminophore oxidation. The absence of a similar peak in the case of **Ru@NP1** is expected in view of their low diffusivity and of the core−shell structure of DDSNs that should unfavor the intimate contact of the redox centers with the electrode surface to permit an efficient electron tunnelling. This leads to low anodic currents that are easily overwhelmed by the water and coreactant oxidation. The availability of dyes embedded in DDSNs for their direct anodic oxidation was on the other hand verified in acetonitrile and in the absence of coreactant so as to minimize the above interference (Figure S16). In line with the results obtained in $Ru(bpy)_3^{2+}$ solutions, we observed in this solvent an anodic signal between 1 and 1.2 V, whose intensity increases with the doping level, that was attributed to the Ru(II) oxidation.

As expected, the ECL profile for **Ru@NP1** displayed a single maximum intensity associated with the coreactant oxidation process, Figure 6b, while a very weak signal was detected in the region of the luminophore oxidation, at odds with the case of free $Ru(bpy)_3^{2+}$ in an analogous solution having the same nominal luminophore concentration (Figure S15). This suggests that the prevailing mechanism for ECL generation is that involving exclusively the electrogenerated coreactant radical cations and radicals according to the scheme below (Scheme 1, showing mechanism I).[1,3,44]

Scheme 1. Mechanism I for the "Oxidative-Reduction" Coreactant ECL Generation[a]

$$\mathbf{DBAE} \rightleftharpoons \mathbf{DBAE^{\bullet+}} + e^- \quad \textbf{(eq. 1)}$$

$$\mathbf{DBAE^{\bullet+}} \rightleftharpoons \mathbf{DBAE^{\bullet}} + H^+ \quad \textbf{(eq. 2)}$$

$$\mathbf{Ru@NP} + \mathbf{DBAE^{\bullet}} \longrightarrow \mathbf{P1} + \mathbf{Ru^{-}@NP} \quad \textbf{(eq. 3)}$$

$$\mathbf{Ru^{-}@NP} + \mathbf{DBAE^{\bullet+}} \longrightarrow \mathbf{DBAE} + \mathbf{Ru^{*}@NP} \quad \textbf{(eq. 4)}$$

$$\mathbf{Ru^{*}@NP} \longrightarrow \mathbf{Ru@NP} + \mathbf{ECL} \quad \textbf{(eq. 5)}$$

[a]DBAE is 2-(dibutylamino)ethanol. **Ru*@NP** is the $Ru(bpy)_3^{2+*}$. **Ru^{-}@NP** is the $Ru(bpy)_3^{+}$. **Ru@NP** is the $Ru(bpy)_3^{2+}$ embedded in the nanoparticle.

At the upper end of the investigated NPs series, **Ru@NP6** (Ru/NP = 24) displayed very different CV and ECL behaviors, somehow specular to those observed in the previous case. Figure 7a,b shows the CV curve and the corresponding ECL profiles measured in an 80 μM **Ru@NP6** solution under similar conditions as in Figure 6.

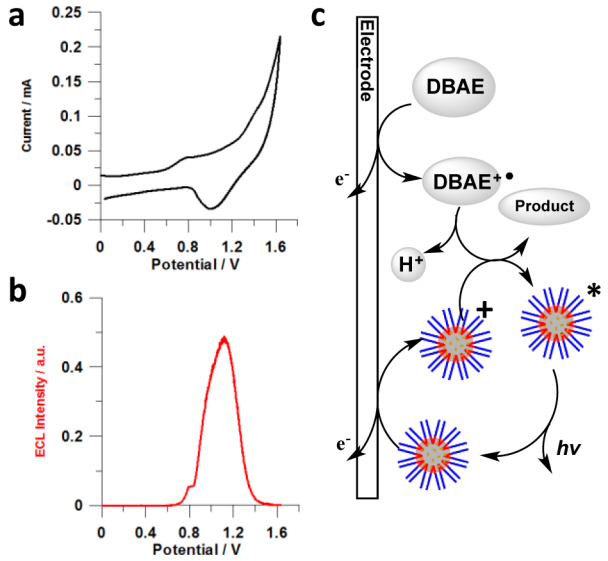

Figure 7. Cyclic voltammetry (black trace panel a) and ECL intensity (red trace panel b) vs potential curves of **Ru@NP6** (Ru/NP = 24), in PB 100 mM solutions, with 30 mM DBAE as coreactant: scan rate 0.1 V s^{-1} (*E* vs SCE), PMT bias 750 V. (c) Schematic representation for mechanism II in the "oxidative-reduction" coreactant homogeneous ECL generation of DDSN and DBAE.

Quite unexpectedly, the anodic peak associated with DBAE oxidation is much less intense than that for **Ru@NP1** (*vide infra*) and is followed, in contrast, by a much more defined and reversible oxidation peak attributable to the direct oxidation of the Ru(II) centers. The ECL profile displays again a single maximum that is however displaced to more positive potentials, in line with the CV pattern, while virtually no emission is recorded in the DBAE oxidation region. The observed behavior would therefore suggest an overall more complex mechanistic scheme than the one outlined above, which would not exclude

DOI: 10.1021/jacs.6b08239
J. Am. Chem. Soc. 2016, 138, 15935−15942

the direct oxidation of the luminophores as a possible route to ECL generation. In a previous study carried out on DDSNs immobilized at the electrode surface,[21] a sizable contribution to ECL generation was proven to derive from electron (hole) hopping between neighboring $Ru(bpy)_3^{2+}$ centers embedded within the NP and following either the direct oxidation of the $Ru(bpy)_3^{2+}$ centers located within a tunnelling distance from the electrode surface or their oxidation by the electrogenerated coreactant radical cations.[37] On the basis of such previous results, we invoke in the present case the following mechanism (Scheme 2, mechanism II), where eqs 6 and 7, that considered the direct oxidation of the $Ru(bpy)_3^{2+}$ centers, replaced eqs 3 and 4 which involve the radical cation of the coreactant.

Scheme 2. Mechanism II for the "Oxidative-Reduction" Coreactant ECL Generation[a]

$$\mathbf{DBAE} \rightleftharpoons \mathbf{DBAE^{\bullet+}} + e^- \quad \textbf{(eq. 1)}$$

$$\mathbf{DBAE^{\bullet+}} \rightleftharpoons \mathbf{DBAE^{\bullet}} + H^+ \quad \textbf{(eq. 2)}$$

$$\mathbf{Ru@NP} \rightleftharpoons \mathbf{Ru^{+}@NP} + e^- \quad \textbf{(eq. 6)}$$

$$\mathbf{DBAE^{\bullet}} + \mathbf{Ru^{+}@NP} \longrightarrow \mathbf{P1} + \mathbf{Ru^{*}@NP} \quad \textbf{(eq. 7)}$$

$$\mathbf{Ru^{*}@NP} \longrightarrow \mathbf{Ru@NP} + \mathbf{ECL} \quad \textbf{(eq. 5)}$$

[a]DBAE is 2-(dibutylamino)ethanol. P1 is the degradation products of DBAE. **Ru*@NP** is the $Ru(bpy)_3^{2+*}$, and **Ru⁺@NP** is the $Ru(bpy)_3^{3+}$ embedded in the nanoparticle.

The efficiency of the hopping mechanism would obviously strongly depend on the average distance between $Ru(bpy)_3^{2+}$ centers and thus on the doping level along the DDSN series.[45] In this way it is possible to explain, at least in part, the different ECL profiles reported above between **Ru@NP1** (Ru−Ru interdistance = 8 nm) and **Ru@NP6** (Ru−Ru interdistance = 3 nm).

Nicely in line with this model, the ECL values of the remaining members of the investigated NPs, with doping levels spanning the range from **Ru@NP1** to **Ru@NP6**, display profiles that gradually evolve from one type to the other shown in Figures 6 and 7, as clearly evidenced in the comparative plot in Figure 8 (**Ru@NP1** to **Ru@NP6**, see also the relative ECL intensities in Figure S17).

While the involvement of the hole hopping mechanism (mechanism II) may in fact explain the birth and growth, along the **Ru@NP1**−**Ru@NP6** series, of the ECL signal in the region of direct Ru(II) oxidation, it can hardly explain the reason for

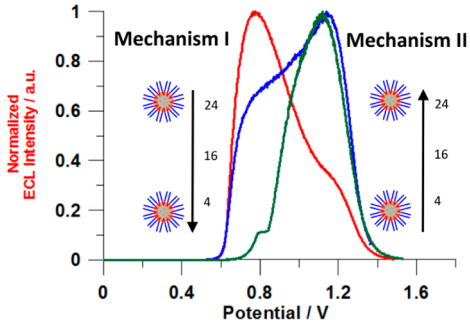

Figure 8. Normalized ECL intensity vs potential curves of **Ru@NP3** (red), **Ru@NP4** (blue), and **Ru@NP6** (green) (Ru/NP = 4, 16, 24) in 100 mM PB solutions, with 30 mM DBAE as coreactant: scan rate 0.1 V s^{-1} (*E* vs SCE), PMT bias 750 V.

the concomitant gradual disappearance of the signal at 0.8 V, promoted by the exclusive coreactant oxidation (mechanism I), whose efficiency should increase, rather than decrease, as the Ru/NP ratio increases. As a matter of fact, it was previously reported in a similar case of the $Ru(bpy)_3^{2+}$/TPA system that the first ECL peak intensity increases steadily with [$Ru(bpy)_3^{2+}$] reaching a plateau for [Ru] > 50 μM (with [TPA] = 100 mM). This is a consequence of the fact that, in a relative excess of $Ru(bpy)_3^{2+}$, the efficiency of the process is governed by the amount of coreactant-based radicals.[44] A similar behavior might then be expected in the present case, although the different dynamics associated with the confined system vis-à-vis the homogeneous case would likely locate the above plateau in a different $Ru(bpy)_3^{2+}$ concentration range. In no case, anyway, should a decrease of the emission be observed, at variance with the experimental evidence which therefore entails additional explanations. In this regard, we noticed that the ζ-potential gradually increases along the DDSN series, as shown in Figure 3, from negative to neutral and finally to slightly positive values. Such a change, in our opinion, may explain the observed decrease and disappearance of the ECL maximum at 0.8 V. As a matter of fact, the coreactant radical cation $DBAE^{\bullet+}$ plays a fundamental role in the mechanism outlined by eqs 1−5, in contrast with that responsible for the emission at 1.2 V (mechanism II), where only the (neutral) DBAE radical is involved. We believe that, as the doping level increases, the decreasing attractive interactions (that turn, at the end, into an increasing repulsion) between the NP and $DBAE^{\bullet+}$ affect negatively the partitioning of the latter inside the hydrophobic shell of DDSNs, thus unfavoring more and more the ECL generation according to mechanism I. Likely due to the decreased repulsive forces between DDSNs is also the observed gradual lowering in the CV curves of the current associated with DBAE oxidation (peak at 0.8 V). Because of their decreasing surface charge, and likely favored by attractive (van der Waals) forces and by their very low diffusivity, DDSNs would in fact form more and more compact layers onto the electrode surface as the Ru/NP ratio increases, that would increasingly hinder coreactant diffusion to the electrode surface thus causing lower oxidation currents. Such a behavior closely resembles the recently reported case of enhanced ECL in thermoresponsive gels;[46] the contribution of the electrocatalytic oxidation of the coreactant by the Ru centers would similarly justify the efficient ECL observed in the highly doped DDSNs even in the presence of a depressed DBAE oxidation current.

The effect of doping on ECL emission was finally quantified by integrating the overall ECL emission (i.e., considering the emission obtained at both potentials) during chronoamperometric experiments with **Ru@NP1−6** carried out at 1.4 V while keeping the same DDSN concentration [**Ru@NP**] = 74 μM, in the presence of 30 mM DBAE (Figure 9 and Figure S18).

Figure 9 shows that, while the ECL intensity generally increases with the number of embedded dyes, a linearity region is only observed in a limited range of Ru/NP ratios, i.e., ≤6, with strong deviations for higher doping levels: in the end, while the number of dyes per particle increases by a factor of 12, the ECL intensity becomes only 5 times higher.

In summary, at low doping levels, where DBAE radical cations are drawn by electrostatic forces inside the DDSNs and mechanism I is therefore fully operative, ECL efficiency increases regularly with the doping level. By contrast, as the DDSN surface charge evolves toward neutral or positive values, the driving force for partitioning DBAE radical cations inside

DOI: 10.1021/jacs.6b08239
J. Am. Chem. Soc. 2016, 138, 15935−15942

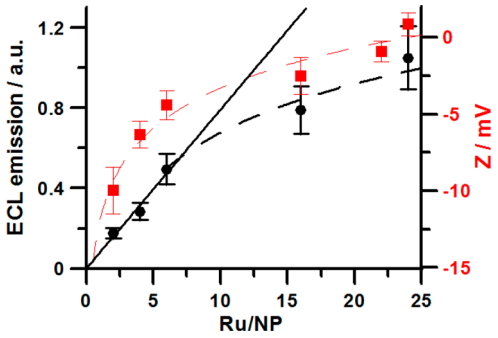

Figure 9. Integrated ECL intensity (black dots) measured during chronamperometric experiments with **Ru@NP1−6** (Ru/NP = 2−24). Conditions: 100 mM PB solutions, 30 mM DBAE as coreactant, applied potential =1.4 V for 0.5 s (*E* vs SCE), PMT bias 750 V, and ζ-potential (red dots) as a function of the doping.

the DDSN ceases thus brings about a severe loss of efficiency of mechanism I. On the other hand, at higher doping levels the probability for hole hopping within the DDSN increases, thus fueling mechanism II. However, this last mechanism does not reach a sufficiently high efficiency to compensate adequately the loss of efficiency in mechanism I, thus explaining the negative deviation from the linear trend.

CONCLUSIONS

The efficiency of ECL generation in covalently doped $Ru(bpy)_3^{2+}$ core−shell silica−PEG NPs depends on various factors that are eventually ascribable to the doping level. While an increase of ECL efficiency is expected upon the covalent accumulation of $Ru(bpy)_3^{2+}$ moieties within the silica core, the concurrent increase of the Ru@NP ζ-potential was found to be detrimental to the activation of the emission events. The observed behavior was attributed to the presence of two different mechanisms for the ECL generation in the DDSNs whose relative contributions would vary as a function of dye density and NPs overall charge, as the latter is able to influence the distribution around/within the NP of charged species involved in the ECL mechanism. The Ru/NP ratio is therefore not the sole parameter requiring optimization in order to increase the brightness of NP-based ECL systems. The reported results, besides contributing to a better understanding of the mechanisms operating in the chemiluminescence generation in nanosystems, also pave the way for the development of very highly efficient ECL labels for ultrasensitive bioanalysis.

ASSOCIATED CONTENT

Supporting Information

The Supporting Information is available free of charge on the ACS Publications website at DOI: 10.1021/jacs.6b08239.

TEM and DLS characterization of **Ru@NP1−6**, ECL from $Ru(bpy)_3^{2+}$, and chronoamperometry ECL experiments for **Ru@NP1−6** (PDF)

AUTHOR INFORMATION

Corresponding Authors

*luca.prodi@unibo.it

*francesco.paolucci@unibo.it

ORCID

Giovanni Valenti: 0000-0002-6223-2072

Present Address

[§]Nanochemistry Laboratory, ISIS & icFRC, Université de Strasbourg & CNRS, 8 allée Gaspard Monge, 67000 Strasbourg, France.

Author Contributions

[‖]G.V. and E. R. contributed equally.

Notes

The authors declare no competing financial interest.

ACKNOWLEDGMENTS

We thank the University of Bologna, Italian Ministero dell'Istruzione, Università e Ricerca (MIUR-project PRIN 2010) and FARB, Fondazione Cassa di Risparmio in Bologna.

REFERENCES

(1) Bard, A. J. *Electrogenerated Chemiluminescence*; Marcel Dekker: New York, 2004.
(2) Miao, W. *Chem. Rev.* **2008**, *108*, 2506−2553.
(3) Liu, Z.; Qi, W.; Xu, G. *Chem. Soc. Rev.* **2015**, *44*, 3117−3142.
(4) Hesari, M.; Ding, Z. *J. Electrochem. Soc.* **2016**, *163* (4), H3116−H3131.
(5) http://www.cobas.com/home/product/clinical-and-immunochemistry-testing/technology-elecsys-ecl.html. (accessed June 28, 2016).
(6) Meso Scale Diagnostics. https://www.mesoscale.com/en/. 2016 (accessed June 28, 2016).
(7) Liu, X.; Shi, L.; Niu, W.; Li, H.; Xu, G. *Angew. Chem., Int. Ed.* **2007**, *46*, 421−424.
(8) Addisu Kitte, S.; Wang, C.; Li, S.; Zholudov, Y.; Qi, L.; Li, J.; Xu, G. *Anal. Bioanal. Chem.* **2016**, *408*, 7059−7065.
(9) Deng, S.; Lei, J.; Huang, Y.; Cheng, Y.; Ju, H. *Anal. Chem.* **2013**, *85*, 5390−5396.
(10) Zamolo, V. A.; Valenti, G.; Venturelli, E.; Chaloin, O.; Marcaccio, M.; Boscolo, S.; Castagnola, V.; Sosa, S.; Berti, F.; Fontanive, G.; Poli, M.; Tubaro, A.; Bianco, A.; Paolucci, F.; Prato, M. *ACS Nano* **2012**, *6*, 7989−7997.
(11) Guo, Z.; Sha, Y.; Hu, Y.; Wang, S. *Chem. Commun.* **2016**, *52*, 4621−4624.
(12) Venkatanarayanan, A.; Crowley, K.; Lestini, E.; Keyes, T. E.; Rusling, J. F.; Forster, R. J. *Biosens. Bioelectron.* **2012**, *31*, 233−239.
(13) Liang, W.; Zhuo, Y.; Xiong, C.; Zheng, Y.; Chai, Y.; Yuan, R. *Anal. Chem.* **2015**, *87*, 12363−12371.
(14) Li, F.; Yu, Y.; Li, Qi; Zhou, M.; Cui, H. *Anal. Chem.* **2014**, *86* (3), 1608−1613.
(15) Valenti, G.; Rampazzo, E.; Biavardi, E.; Villani, E.; Fracasso, G.; Marcaccio, M.; Bertani, F.; Ramarli, D.; Dalcanale, E.; Paolucci, F.; Prodi, L. *Faraday Discuss.* **2015**, *185*, 299−309.
(16) Bonacchi, S.; Genovese, D.; Juris, R.; Montalti, M.; Prodi, L.; Rampazzo, E.; Zaccheroni, N. *Angew. Chem., Int. Ed.* **2011**, *50*, 4056−4066.
(17) Montalti, M.; Prodi, L.; Rampazzo, E.; Zaccheroni, N. *Chem. Soc. Rev.* **2014**, *43*, 4243−4268.
(18) Dong, Y.-P.; Chen, G.; Zhou, Y.; Zhu, J.-J. *Anal. Chem.* **2016**, *88*, 1922−1929.
(19) Wusimanjiang, Y.; Meyer, A.; Lu, L.; Miao, W. *Anal. Bioanal. Chem.* **2016**, *408*, 7049−7057.
(20) Zhao, P.; Zhou, L.; Nie, Z.; Xu, X.; Li, W.; Huang, Y.; He, K.; Yao, S. *Anal. Chem.* **2013**, *85*, 6279−6286.
(21) Sun, H.; Ma, S.; Li, Y.; Qi, H.; Ning, X.; Zheng, J. *Biosens. Bioelectron.* **2016**, *79*, 92−97.
(22) Dai, R.; Wu, F.; Xu, H.; Chi, Y. *ACS Appl. Mater. Interfaces* **2015**, *7*, 15160−15167.
(23) Chen, H.; Lu, Q.; Liao, J.; Yuan, R.; Chen, S. *Chem. Commun.* **2016**, *52*, 7276−7279.
(24) Qi, H.; Zhang, C.; Huang, Z.; Wang, L.; Wang, W.; Bard, A. J. *J. Am. Chem. Soc.* **2016**, *138*, 1947−1954.

DOI: 10.1021/jacs.6b08239
J. Am. Chem. Soc. 2016, 138, 15935−15942

(25) Li, H.; Daniel, J.; Verlhac, J.-B.; Blanchard-Desce, M.; Sojic, N. *Chem. - Eur. J.* **2016**, *22*, 12702.
(26) Wang, X.-d.; Stolwijk, J. A.; Lang, T.; Sperber, M.; Meier, R. J.; Wegener, J.; Wolfbeis, O. S. *J. Am. Chem. Soc.* **2012**, *134*, 17011−17014.
(27) Zanarini, S.; Rampazzo, E.; Bonacchi, S.; Juris, R.; Marcaccio, M.; Montalti, M.; Paolucci, F.; Prodi, L. *J. Am. Chem. Soc.* **2009**, *131*, 14208−14209.
(28) Zanarini, S.; Rampazzo, E.; Ciana, L. D.; Marcaccio, M.; Marzocchi, E.; Montalti, M.; Paolucci, F.; Prodi, L. *J. Am. Chem. Soc.* **2009**, *131*, 2260−2267.
(29) Valenti, G.; Rampazzo, E.; Bonacchi, S.; Khajvand, T.; Juris, R.; Montalti, M.; Marcaccio, M.; Paolucci, F.; Prodi, L. *Chem. Commun.* **2012**, *48*, 4187−4189.
(30) Qi, W.; Wu, D.; Zhao, J.; Liu, Z.; Zhang, W.; Zhang, L.; Xu, G. *Anal. Chem.* **2013**, *85*, 3207−3212.
(31) Pinaud, F.; Millereux, R.; Vialar-Trarieux, P.; Catargi, B.; Pinet, S.; Gosse, I.; Sojic, N.; Ravaine, V. *J. Phys. Chem. B* **2015**, *119*, 12954−12961.
(32) Bagwe, R. P.; Hilliard, L. R.; Tan, W. *Langmuir* **2006**, *22*, 4357−4362.
(33) Wang, D.; Guo, L.; Huang, R.; Qiu, B.; Lin, Z.; Chen, G. *Sci. Rep.* **2015**, *5*, 7954.
(34) Zanarini, S.; Rampazzo, E.; Bich, D.; Canteri, R.; Della Ciana, L.; Marcaccio, M.; Marzocchi, E.; Montalti, M.; Panciatichi, C.; Pederzolli, C.; Paolucci, F.; Prodi, L.; Vanzetti, L. *J. Phys. Chem. C* **2008**, *112*, 2949−2957.
(35) Della Ciana, L.; Hamachi, I.; Meyer, T. J. *J. Org. Chem.* **1989**, *54*, 1731−1735.
(36) Montalti, M.; Credi, A.; Prodi, L.; Gandolfi, M. T. *Handbook of Photochemistry*, 3rd ed.; CRC Taylor & Francis: Boca Raton, FL, 2006.
(37) Valenti, G.; Zangheri, M.; Sansaloni, S. E.; Mirasoli, M.; Penicaud, A.; Roda, A.; Paolucci, F. *Chem. - Eur. J.* **2015**, *21*, 12640−12645.
(38) Genovese, D.; Bonacchi, S.; Juris, R.; Montalti, M.; Prodi, L.; Rampazzo, E.; Zaccheroni, N. *Angew. Chem., Int. Ed.* **2013**, *52*, 5965−5968.
(39) Rampazzo, E.; Bonacchi, S.; Genovese, D.; Juris, R.; Montalti, M.; Paterlini, V.; Zaccheroni, N.; Dumas-Verdes, C.; Clavier, G.; Méallet-Renault, R.; Prodi, L. *J. Phys. Chem. C* **2014**, *118*, 9261−9267.
(40) Helle, M.; Rampazzo, E.; Monchanin, M.; Marchal, F.; Guillemin, F.; Bonacchi, S.; Salis, F.; Prodi, L.; Bezdetnaya, L. *ACS Nano* **2013**, *7*, 8645−57.
(41) Rampazzo, E.; Voltan, R.; Petrizza, L.; Zaccheroni, N.; Prodi, L.; Casciano, F.; Zauli, G.; Secchiero, P. *Nanoscale* **2013**, *5*, 7897−905.
(42) Genovese, D.; Rampazzo, E.; Bonacchi, S.; Montalti, M.; Zaccheroni, N.; Prodi, L. *Nanoscale* **2014**, *6*, 3022−3036.
(43) Rampazzo, E.; Bonacchi, S.; Montalti, M.; Prodi, L.; Zaccheroni, N. *J. Am. Chem. Soc.* **2007**, *129*, 14251−14256.
(44) Miao, W.; Choi, J.-P.; Bard, A. J. *J. Am. Chem. Soc.* **2002**, *124*, 14478−14485.
(45) Imai, K.; Valenti, G.; Villani, E.; Rapino, S.; Rampazzo, E.; Marcaccio, M.; Prodi, L.; Paolucci, F. *J. Phys. Chem. C* **2015**, *119*, 26111−26118.
(46) Pinaud, F.; Russo, L.; Pinet, S.; Gosse, I.; Ravaine, V.; Sojic, N. *J. Am. Chem. Soc.* **2013**, *135*, 5517−5520.

DOI: 10.1021/jacs.6b08239
J. Am. Chem. Soc. 2016, 138, 15935−15942